Front. Earth Sci. 2023, 17(3): 701−712
https://doi.org/10.1007/s11707-022-1060-8

RESEARCH ARTICLE

Coal and rock dynamic disaster prevention and control technology in the large mining face of a deep outburst mine

Jianguo ZHANG[1], Man WANG[1], Hongwei ZHOU[4], Dongming ZHANG (✉)[2,3], Beichen YU[2,3], Chongyang WANG[2,3], Yujie WANG[1]

1 State Key Laboratory of Coking Coal Exploitation and Comprehensive Utilization, China Pingmei Shenma Holding Group CO., LTD, Pingdingshan 467000, China
2 State Key Laboratory of Coal Mine Disaster Dynamics and Control, Chongqing University, Chongqing 400030, China
3 School of Resources and Safety Engineering, Chongqing University, Chongqing 400030, China
4 School of Energy and Mining Engineering, China University of Mining and Technology (Beijing), Beijing 100083, China

Abstract In this study, we systematically studied the occurrence regularity of *in situ* stress in the Pingdingshan mine. The critical criterion model of coal-rock destabilization was established based on the theoretical framework of fracture mechanics. Furthermore, we analyzed the coupling destabilization mechanism of *in situ* stress and gas and studied the influence of the variation between original rock stress and mining-induced stress on the critical criterion. Through field experiments and applications, we established a three-dimensional gas drainage technology system for areas with a large mining height and long work face. Based on our research, a demonstration project was developed for deep mine dynamic disaster control. The technical system included the arrangement and optimization of pre-drainage holes along the coal seam, technology, and optimization of gas drainage through the bottom drainage tunnel and upper corner, gas drainage technology through sieve tubes, and a two plugging with one injection under pressure sealing technology. The implementation of the demonstration project effectively reduced the gas content and pressure of the coal seam in the deep mine, and the project increased the critical strength of the instability and failure of coal and rock.

Keywords *in-situ* stress, dynamic disaster, critical criterion, gas drainage

1 Introduction

Currently, two mining modes exist in coal mine production, open-pit mining and well mining. Most coal mines in coal seams are underground mines. Owing to the increasing demand for coal resources, both mining depth and mining intensity have been increased. Consequently, the geological conditions of a coal seam have become increasingly complex, leading to the frequent occurrence of coal and rock dynamic disasters (Zhang, 2015; Liu et al., 2022). Gas disaster is an important factor that restricts the safe and efficient production of a mine. The *in situ* stress, gas pressure, and ground temperature in the coal seam increase with increasing mining depth. The current mining depth of the Pingdingshan mining area is 800 m, and is associated with high gas content, low gas permeability, and high outburst risk. Mine geological conditions, gas occurrence conditions, and coal mining technologies have changed with the development of deep mining. With the increase in mining depth from −400 m to −800 m in the Pingdingshan mining area, the gas pressure of the coal seam has increased from 1.67 MPa to 2.45 MPa, and the gas content of the coal seam has increased from 11.56 m^3/t to 27.2 m^3/t. A positive correlation is observed between the gas pressure and the buried depth (Zhang et al., 2019).

The rise of coal seam gas pressure and content increases the risk of coal and gas outburst. Coal and rock dynamic disasters are multi-factor, coupled disaster phenomena with high gas pressure, high *in situ* stress, and low permeability of coal and rock. Some researchers have conducted in-depth studies on dynamic disasters in deep coal mining. Qi et al. (2018) proposed the idea of multi-scale and multi-source prevention and control of dynamic disasters in deep coal mining. They proposed that the prevention and control of dynamic disasters in coal mines mainly adopted the joint region-local prevention and control method of upper and lower wells, and that the

Received August 11, 2022; accepted November 29, 2022

E-mail: zhangdm@cqu.edu.cn

main control factor was the gas source. Li et al. (2020) studied the efficient mining technology system of coal and gas outburst and proposed a variety of coal and gas co-mining modes. Zhu et al. (2017) analyzed the influencing factors of coal mine dynamic disasters and classified dynamic disasters based on the energy release. Long and large mining height work face mining technology was adopted in the deep mining area of Pingdingshan. This high-intensity mining technology made the mechanism of coal-rock dynamic disaster more complicated, and negatively impacted the safety and efficient production of the coal mine. In this study, we examined the coal and rock instability failure mechanism involving gas pressure for deep mines and large mining height work faces, demonstrated a proposed technology for coal and rock dynamic disaster prevention and control, and described the control effect.

2 Study area overview

The Pingdingshan mining area is greatly influenced by geological structure, and the coal seam fluctuates, indicating that the spatial distribution states of multiple anticlines and synclines are interactively connected. The stress concentration area is large, and the stress distribution of the entire coalfield is not uniform. The first coal and gas outburst accident in the Pingdingshan mining area occurred in 1984, with 157 incidents in total. The average amount of coal outburst and gas emission per incident is 117.2 ton and 8633.6 m^3, respectively. With the increased demand for mineral resources, deep mining has been initiated in the Shoushan and No. 12 mines in the Pingdingshan mining area. The gas pressure and content in the coal seam has increased owing to the gradual deterioration of coal mining geological conditions and the work environment under deep mining. Consequently, dynamic coal and gas outburst disasters in the mines have become increasingly severe. These factors create new challenges and requirements for dynamic coal mine disaster prevention and control (Whittaker et al., 1992).

3 Fracture regularity and influencing factors of deep rock mass

Under deep mining conditions, the coal and rock mass are subjected to an environment with high *in situ* stress, gas pressure, and stress disturbance. Although deep coal and rock are subjected to high *in situ* stress, the mining process follows the spatial stress variation influenced by mining. Current studies show that an increase in mining depth leads to the coal body reaching the initial strength and plastic limit due to its low strength and stiffness, leading to brittle-plastic transformation. The coal body is prone to chip, impact, and large plastic deformation under mining action (Xie et al., 2015). Furthermore, internal cracks continue to develop in the rock mass due to *in situ* stress and deep mining-induced stress, and its mechanical and seepage characteristics are important with regard to deep roadway excavation, support, and stability control (Zhang and Song, 2020). Therefore, establishing the failure criterion based on high *in situ* stress, which is caused by mining-induced fracture development in coal and rock mass under deep mining conditions, is necessary in deep mining.

3.1 Instability failure criterion of deep rock mass

The development of rock fractures is exacerbated by high *in situ* stress and strong mining disturbance during deep mining, and rock mass fracturing and swelling occur frequently. According to the fracture toughness theory of elastic-brittle materials, mining-induced fractures in rock mass mainly undergo slip failure (Deng et al., 2012). According to the condition of mining-induced fracture propagation, the stress intensity factor reaches the critical state $|K_{II}| = K_{IIc}$, where K_{IIc} is the fracture toughness of type II cracks, and is the material characteristic constant. According to the maximum circumferential theory, $K_{IIc}/K_{Ic} = \sqrt{3}/2$, K_{Ic} is the fracture toughness of type I cracks, and is the material constant that can be measured experimentally. The calculation formula of K_{IIc} can be expressed as follows:

$$K_{IIc} = \frac{p_1}{2}\left[\sin 2\beta - f\left(1-\cos 2\beta\right)\right]\sqrt{\pi a}. \tag{1}$$

Critical load $p_1 = \sigma_c$. The fracture ability of roof and floor rock in the coal seam is $k_{cr} = \sigma_c\sqrt{\pi a}$ when coupled with Eq. (1):

$$k_{cr} = \frac{2K_{IIc}}{\sin 2\beta - f\left(1-\cos 2\beta\right)}, \tag{2}$$

where f is the friction coefficient on the crack surface, β is the angle of the micro-crack (the angle between the crack and the vertical direction) and k_{cr} is the function of f and β. It is assumed that the frictional properties of cracks are uniformly distributed, that is, f is constant. According to the above analysis, β can be used as an independent variable to study k_{cr} by changing the inclination angle of the fracture ($90°-\beta$) and analyzing the evolution of k_{cr}. From 0°to 90°, k_{cr} has a minimum value and two infinite asymptotic values denoted as k_{crmin}, and the inclination angle of the fracture at this time is β_c. This fracture is the priority fracture under true triaxial mining-induced stress (Zhang et al., 1998; Gong et al., 2014; Liu et al., 2018; Lu, 2018). When k_{cr} reaches a minimum value:

$$\frac{\partial k_{cr}}{\partial \beta} = -\frac{4K_{IIc}\left(\cos 2\beta - f\sin\beta\right)}{\left[\sin 2\beta - f\left(1-\cos 2\beta\right)\right]^2} = 0. \tag{3}$$

Therefore, Eq. (3) shows $\cos 2\beta - f\sin\beta = 0$.

Solution of the $\beta_c = \frac{1}{2}\tan^{-1}\frac{1}{f}$, $\sin 2\beta = \frac{1}{\sqrt{1+f^2}}$, $\cos 2\beta = \frac{f}{\sqrt{1+f^2}}$, substituting it into k_{cr} obtains:

$$k_{cr} = \frac{2K_{IIc}}{\sqrt{1+f^2}-f}. \tag{4}$$

Equation (4) can be expressed as:

$$k_{cr} = 2K_{IIc}\left(\sqrt{1+f^2}+f\right). \tag{5}$$

Currently, the critical stress is σ_c:

$$\sigma_c = \frac{2K_{IIc}\left(\sqrt{1+f^2}+f\right)}{\sqrt{\pi a}}. \tag{6}$$

According to the maximum circumferential theory, Eq. (6) can be transformed into the expression of fracture toughness K_{Ic} of type I cracks. As shown below, the K_{Ic} of the *in situ* rock mass can be measured by experiments:

$$\sigma_c = \frac{\sqrt{3}K_{Ic}\left(\sqrt{1+f^2}+f\right)}{\sqrt{\pi a}}. \tag{7}$$

The American Society for Testing Materials specification has put forward a formula for the determination of type I fracture toughness using a three-point bending test (Srawley and Brown, 1965; ASTM, 1983; Cao, 2009):

$$K_{Ic} = \frac{3PS}{2BW}\left[1.99 - \frac{a}{W}\left(1-\frac{a}{W}\right)\left(2.15 - 3.93\frac{a}{W} + 2.7\frac{a^2}{W^2}\right)\right] / \left(1+2\frac{a}{W}\right)\left(1-\frac{a}{W}\right)^{\frac{3}{2}}. \tag{8}$$

In 2014, the International Society of Rock Mechanics proposed the "Test Method for Fracture Toughness of Central slotted Three-point bending Semi-disk Specimens (SCB method)" (Ma et al., 2019). Compared to other methods, the SCB method requires smaller specimens and can be easily implemented on site. The experiment can be performed easily and is an ideal method for testing rock fracture toughness. The following calculation formula can be applied if the SCB test method is adopted (Kuruppu et al., 2014):

$$K_{Ic} = \frac{P_{max}\sqrt{\pi a}}{2RB}Y', \tag{9}$$

where K_{Ic} is type I fracture toughness; P_{max} is the load when the sample was broken; B is the thickness of the sample; S is the distance between two ends; a is the length of manual cutting groove; R is the radius of SCB sample; $Y' = -1.297 + 9.516\left(\frac{S}{2R}\right) - \left[0.47 + 16.457\left(\frac{S}{2R}\right)\right]\beta + \left[1.071 + 34.401\left(\frac{S}{2R}\right)\right]\beta^2$; $\beta = a/R$.

The critical stress state of rock mass, σ_c, represents the critical stress of rock mass instability and failure under mining action. When the stress exceeds σ_c, the rock mass can be elastic-brittle damaged, resulting in dynamic load before the induction of dynamic disaster.

3.2 Deviatoric stress criterion for instability failure of deep coal

Deep mining under high stress conditions increases the likelihood of coal and gas outburst and other dynamic disasters. In a previous study, we conducted a long-term systematic investigation of the *in situ* stress in the Pingdingshan mining area (Tian et al., 2008). The results showed that the maximum principal stress in the area is close to the horizontal state. The ratio of the maximum horizontal principal stress, σ_H, to the vertical principal stress, σ_v, ranges from 1.6 to 2.8, and the average volumetric weight of the overlying strata is γ=25 kN/m^3. Below 1000 m, the maximum principal stress reaches 40–50 MPa and the local high stress area exceeds 60 MPa. The direction of σ_H is mainly NE-SW.

The minimum principal stress, σ_h, is close to the horizontal direction, and the difference between the two principal stresses in the horizontal direction is large. Comparisons between the maximum and minimum horizontal principal stresses of some test points are shown in Table 1. The uneven distribution of *in situ* stress subjects the underground coal and rock to bias pressure, which poses a major threat to mining activities.

Because the cracking failure of type II fractures in coal and rock mass is mainly related to the deviatoric stress of coal and rock mass, the stress intensity factor of type II fracture can be obtained by considering the spherical stress and the deviatoric stress, τ ($\frac{\sigma_H - \sigma_h}{2}$), and gas pressure, P_0:

$$\begin{aligned} K_{II} &= [\tau - f(P - P_0)]\sqrt{\pi a}, \\ K_{II} &= \left[\frac{\sigma_H - \sigma_h}{2} - f(P - P_0)\right]\sqrt{\pi a}, \\ K_{II} &= \left[\frac{\sigma_H - \sigma_h}{2} - f\left(\frac{\sigma_H + \sigma_h + \sigma_v}{3} - P_0\right)\right]\sqrt{\pi a}. \end{aligned} \tag{10}$$

Thus, the critical criterion of elastic-brittle failure of

Table 1 Ratio of maximum and minimum horizontal principal stresses of some measuring points in Pingdingshan mining area

Point	1	2	3	4	5	6	7	8	9	10	11
σ_H/σ_h	2.09	1.93	1.82	1.88	1.90	1.74	1.70	2.04	1.60	1.42	1.88

rock mass under *in situ* stress can be expressed as follows:

$$\sigma_c = 2\left[\frac{\sigma_H - \sigma_h}{2} - f\left(\frac{\sigma_H + \sigma_h + \sigma_v}{3} - P_0\right)\right]\left(\sqrt{1+f^2}+f\right). \tag{11}$$

The gradient of gas pressure development from the shallow to deep stratum (increasing gas pressure per meter) is generally 0.01 ± 0.005 and the temporary value is 0.005 in this study (Kang, 2013). This gas pressure gradient is close to the gas occurrence state in the Pingdingshan mining area. According to this gas pressure gradient, the gas pressure reached approximately 4 MPa at a depth of 800 m. With the value of f being constant at 0.5, the unstable failure of different deep coal and rock mass was analyzed according to Eq. (10). Figure 1 shows the distribution of *in situ* stress at different depths and the variation in critical criterion of deviatoric stress of coal and rock instability failure along different mining depths.

Based on the linear fitting of the data in Fig. 1, the variation in maximum horizontal principal stress, minimum horizontal principal stress, and vertical principal stress with depth can be obtained as is shown in equations below:

$$\begin{cases} \sigma_H = 4.89x + 0.04,\ R^2 = 0.99 \\ \sigma_h = 2.76x + 0.69,\ R^2 = 0.98 \\ \sigma_v = 2.69x + 0.01,\ R^2 = 0.99 \end{cases}. \tag{12}$$

3.3 Influence of mining stress on critical criterion of rock mass

The stress field of the original rock in the work face changed with the advance of the work face. The stress in the coal and rock mass changed dynamically, causing the stress concentration area of the coal body to move in front of the work face, while the direction of the goaf presented the pressure relief area. According to the results of previous studies, the mining stress in the coal body in front of the mining face increased to 2–5 times the original rock stress and the pressure relief coefficient, λ ($\lambda = \frac{p_{initial} - p_{reduced}}{p_{initial}}$), of the roof and floor pressure relief zone of the goaf reduced to 0.4. Figure 2 shows the schematic diagram of mining stress distribution in the mining face. In the Figure, k_1 and k_2 are the stress concentration coefficients (coefficients with values larger than 1) on the work face and H is the buried depth of the coal seam. γ is the average bulk density of the overlying strata of the coal seam, s_1 and s_2 are the position parameters of the peak of abutment pressure in the working face, h is the stress state of a certain rock mass in the surrounding rock and the vertical distance from the coal seam floor, and b is the horizontal distance from the coal wall of the working face. The stress state of a point in the coal floor is affected by the buried depth and the abutment pressure distribution of the coal wall in the work face (Fig. 2).

According to the analysis shown in Fig. 2, the origin of coordinates is located in the upper strata of the coal wall, with the x axis in the vertical direction and the y axis in the horizontal direction. To study the distribution of the stress field in the coal seam of the working face and floor surrounding the rock mass, the micro-element, $d\xi$, is taken at a distance ξ from the origin, and the stress of this micro-element body is $qd\xi$. The analytical formula of the stress component at $M(h,b)$ points of the floor surrounding the rock mass is as follows (Zhang et al., 2008):

$$d\sigma_x = -\frac{2qd\xi}{\pi}\frac{h^3}{\left[h^2+(b-\xi)^2\right]^2}, \tag{13}$$

$$d\sigma_y = -\frac{2qd\xi}{\pi}\frac{h(b-\xi)^2}{\left[h^2+(b-\xi)^2\right]^2}, \tag{14}$$

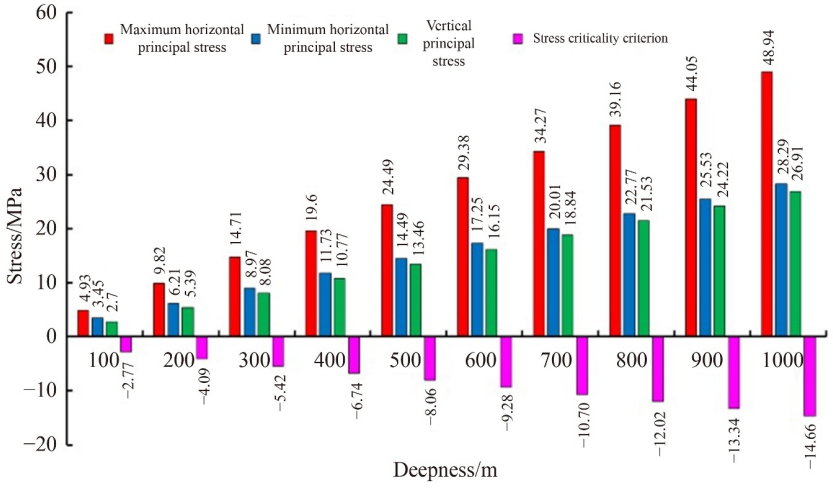

Fig. 1 Critical criterion of *in situ* stress and stress at different depths.

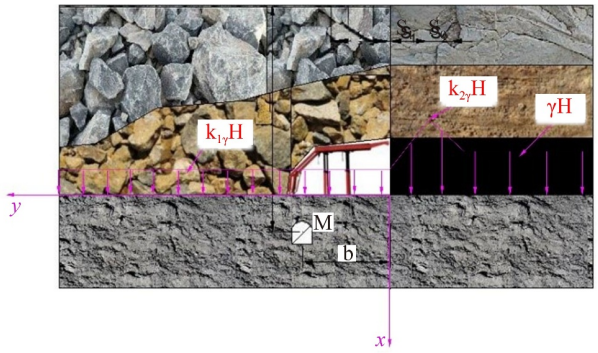

Fig. 2 Stress field analysis of surrounding rock.

$$d\tau_{xy} = -\frac{2qd\xi}{\pi}\frac{h^2(b-\xi)}{\left[h^2+(b-\xi)^2\right]^2}, \quad (15)$$

where σ_x is the vertical stress at point M; σ_y is the horizontal stress at point M; τ_{xy} is the shear stress at point M.

By substituting the results calculated in Eqs. (13−15) into Eq. (12), the critical criterion of coal and rock mass instability under mining stress can also be obtained, which cannot be repeated here. The work face mining stress concentration on the influence of critical stress index under constant gas pressure is shown in Fig. 3. The coal and rock in front of the work face occurred the stress concentration and the vertical stress increased by the initial stress state to mining stress. The critical instability and failure of coal and rock stress improved as well, and the curve slope showed a value of 11.61.

The mining pressure relief zone was located at a certain distance behind the coal wall of the work face. Figure 4 shows the influence of the pressure relief coefficient of coal and rock mass on critical stress. Its slope is 13.78, which is larger than that of the relation curve between the stress concentration coefficient and the critical pressure. This shows that the pressure relief of the coal and rock mass has a major influence on the stability of coal and rock mass. The fracture of coal and rock mass first appeared in the pressure relief area.

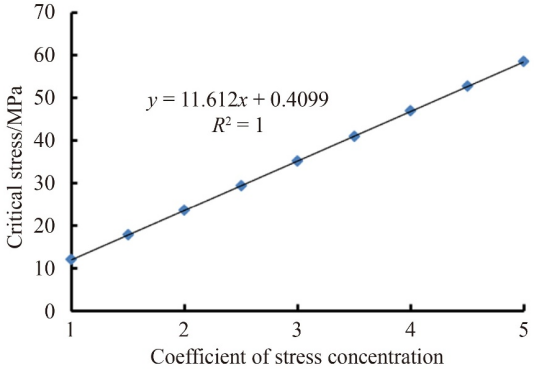

Fig. 3 Relationship between the stress concentration coefficient and critical stress in the working face.

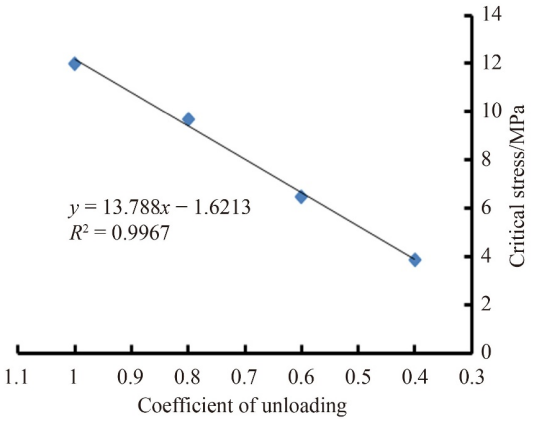

Fig. 4 Relationship between mining pressure relief and critical stress.

3.4 Influence of gas pressure on critical criterion of coal mass

The critical failure strength of coal and rock mass is greatly affected by gas pressure, and the existence of gas pressure exacerbates its weakening. Taking the depth of 800 m as an example, the maximum and minimum principal stresses at this depth are 39.16 and 21.53 MPa, respectively. Under these stress conditions, the stress values decrease as gas pressure increases. Figure 5 shows the deterioration of the failure criterion of coal and rock mass with the increase in gas pressure at 800 m. According to the analysis shown in Fig. 5, when the gas pressure is zero, the failure criterion of coal and rock mass is 18.49 MPa, while the actual gas pressure is 4 MPa. When the failure criterion of coal and rock mass becomes 12.02 MPa, resulting in 35% strength deterioration. Gas pressure is very unfavorable to coal and rock mass stability. The increase in pore pressure could enhance shear sliding in the brittle regime and promote shear fracture development, which could accelerate damage. As bedding and cleats exist in coal, fractures tend to propagate along and then penetrate the bedding plane, which eventually accelerates fracture propagation along the bedding direction from the fracture tip until tensile damage occurs.

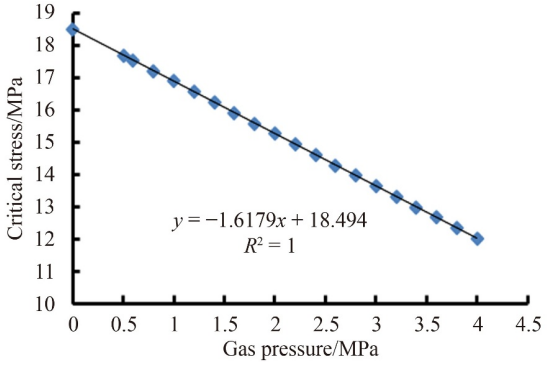

Fig. 5 Deterioration of failure criterion with the increase in gas pressure.

Gas pressure on the depth of different critical strength of coal and rock is shown in Fig. 6. The influence of different depths on the gas pressure gradient change depends upon the gas, with other conditions being the same as those mentioned above. The contrast curve is calculated under a gas pressure of 0.5 MPa. The coal and rock strength in the low gas pressure area are much higher than those in the high gas pressure area. The effect of gas pressure on the strength deterioration of coal and rock mass increases linearly with depth.

The higher the gas pressure, the easier it is to produce instability failure in coal and rock masses at different depths. Therefore, to ensure safe and efficient mining of deep well and high outburst coal seams, effective measures must be taken to reduce the occurrence of dynamic disasters by reducing gas pressure and improving the strength of coal and rock mass.

4 Three-dimension gas extraction technology of deep mining coal seam

Considering the influence of mining stress and coal seam gas pressure on the critical stress criterion of rock mass, the gas disaster management under deep mining conditions should ensure the strength of rock mass and reduce the gas pressure to the farthest possible extent.

Taking the deep mining face of Shoushan No. 1 Mine in the Pingdingshan mining area as the focus of this study, and in view of the large buried depth of the fully mechanized work face, 12090, we set the location of the pumping roadway and distribution of pumping drilling holes based on the failure criterion of the coal and rock mass. The mining strike length of the work face 12090 was set to 1536 m, the mining length to 256 m, and the mining height to 6 m. The gas pressure and content in the coal seam is high owing to the influence of factors such as the large depth of the coal seam and its complex geological structure. The maximum measured original gas content of the coal seam in the work face is 10.46 m^3/t.

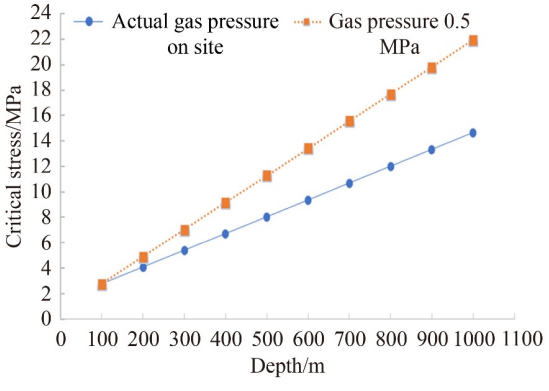

Fig. 6 Deterioration of coal and rock mass strength in different depth by gas pressure.

Based on the critical stress of roadway surrounding rock failure, we proposed and optimized the comprehensive gas control technology of "one side and multiple lanes", optimized the layout parameters, and determined the effective extraction radius of gas pre-drainage boreholes. Additionally, we optimized the pressure relief gas drainage technology based on a high drainage roadway and investigated the drainage effect. Moreover, field tests were conducted on the devolved screen pipe gas extraction technology using a two plugging and one injection with pressure sealing process. The corresponding construction method was optimized. Thus, the extraction technology for a large mining height and long face of a coal seam gas system and the deep mine dynamic disaster management project were established. This effectively reduced the coalbed gas content and pressure, increased the instability and failure of coal and rock critical strength, and reduced the dynamic disaster risk, which played an essential role in solving the corresponding problems of other mines.

4.1 One side multilane gas area management project layout

The present study focused on the Shoushan No. 1 mine located in the east section of the Pingdingshan mining area. The main structure of the well field is a wide and gentle anticline known as the Baishishan anticline. The stratigraphic strike is generally 290°–320°. Fourteen faults have been identified in the mine field, most of which are located in the west. The other areas have few faults, of which only one normal and one reverse fault are developed near the Baishishan anticline axis to the east of the mine field. Further, a preliminary geological report predicted that the No. 2 and No. 3 coal seams possess an outburst danger.

In the Shoushan mine, the traditional one side and four lanes are used for gas regional control in the early stage. The mine is 150 m long and comprises 2 coal and 2 rock lanes. There are frequent replacements in the work place. Although the problems of regional outburst prevention are solved preliminarily, mining height, and working face length also increased with mining depth, which caused the coal seam gas content to increase. The original gas treatment method is not effective for the gas treatment of the ultra-long work face.

After a long and systematic study, the coal seam gas control technology of one side with seven lanes was put forward considering the deep large mining height face of Shoushan No. 1 mine as the specific engineering background. The traditional roadway arrangement of the mining face consisted of an air inlet lane and air return lane. In some coal mines, the mining face has a middle coal roadway arrangement. Based on the original design, this study added a gas drainage lane for the air, transportation, and medium coal roadways. The gas drainage lane and medium coal roadway doubled as the

air inlet lane. The gas in the corner of the deep mining face and the gas in the goaf substantially affect the progress of the working face; therefore, the high drainage roadway was designed and optimized to efficiently drain the gas in the upper corner and the goaf. Through the optimized layout of the roadway mentioned above, a three-dimensional pumping system of one side and seven lanes was created (Fig. 7). The mining face of the Shoushan mine is a single, large, long coal mining face with outbursts in the deep area. Using a stereo extraction technology with seven lanes on the mountain improved the shortage problems of excavating and taking over, and shortened the time of gas extraction from the coal seam, which made the gas content of the coal seam fall below

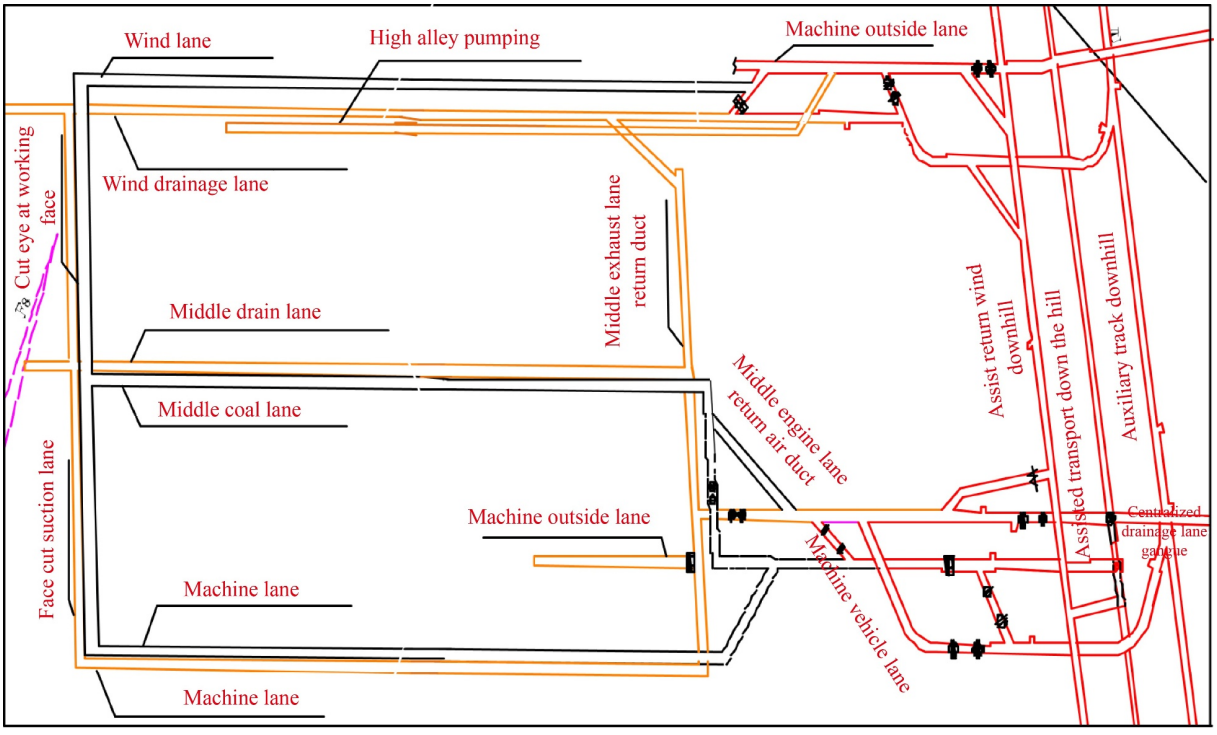

(a)

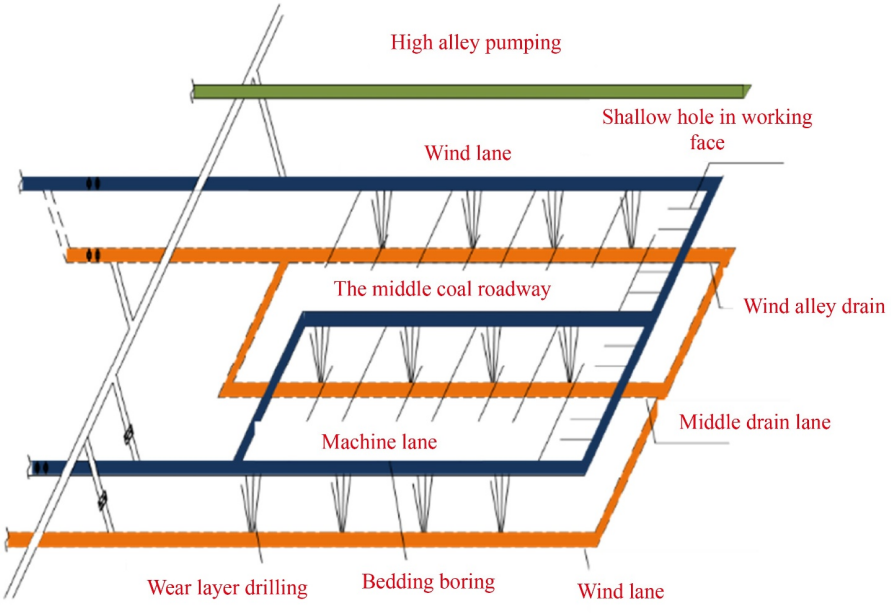

(b)

Fig. 7 Schematic diagram of the one side, seven lane three-dimensional gas drainage system layout. (a) Plane diagram. (b) Three-dimensional diagram.

the critical value. This eliminated the outburst risk of the coal seam and guaranteed the safety of underground production.

4.2 Principle of three-dimensional gas extraction in a deep mining face

With the aim of controlling gas in the outburst coal work face in the deep area, we studied and implemented the multi-source gas three-dimensional extraction technology. The stereoscopic gas extraction technology of drilling pre-drainage through strata in low drainage roadway-pressure relief and closure drainage, drilling pre-drainage along strata-pressure relief and enhanced drainage, and closed drainage in high drainage roadways was established. Additionally, a comprehensive anti-outburst gas extraction system for work faces with dangerous outbursts in deep mines has been developed. The comprehensive pipeline system for stereoscopic gas extraction is shown in Fig. 8.

4.3 Application of three-dimension gas extraction technology in deep mining faces

To study the effect of coal seam gas extraction, we studied the gas extraction rate of pre-drainage boreholes. The influencing factors of gas extraction rate include the gas permeability of the coal seam, initial extraction amount of a 100 m borehole, attenuation coefficient of gas extraction from the borehole, density of the borehole, depth of the borehole, and the original gas content of the coal body. Taking the above factors into consideration, the gas pre-drainage rate of a borehole is defined as follows (Yan, 2010):

$$\eta_t = \frac{\left[1.44 q_{c0}\left(1-e^{-\beta t}\right)/\beta\right] L_1}{W_0 (L_0 - d_1) M_0 \cdot r \cdot z}, \tag{16}$$

where η_s is the borehole gas extraction rate, %; q_{c0} is the initial extraction volume of a 100-m borehole, m^3/min.hm; β is the attenuation coefficient of the borehole gas extraction, d^{-1}; t is the mean borehole extraction time, d; L_1 is the average hole depth of drilling, m; W_0 is the original gas content of the coal, m^3/t; L_0 is the working face strikes length, m; d_1 is the equivalent width of road pre-drainage gas, m; M_0 is the coal thickness, m; r is the density of the coal, t/m^3; and z is the distance between extraction holes, m.

We determined the target residual gas content index to be 6 m^3/t in the measurement of coal seam gas pre-drainage in work face 12090. The measured original coal seam gas content in the test area was found to be 9.59 m^3/t and the gas pre-drainage rate reached 37.4%. Four groups of boreholes with different spacings were drilled into the work face. Based on the monitoring data, the relationship between the pre-pumping rate and the pumping time were obtained as shown in Fig. 9.

The technical index of work face 12090 was determined through field testing and research. Following the application of this technology, when the hole spacing was 1.6 m and the negative pressure was 13–16 kPa, the extraction time could reach the standard in approximately 80–87 days.

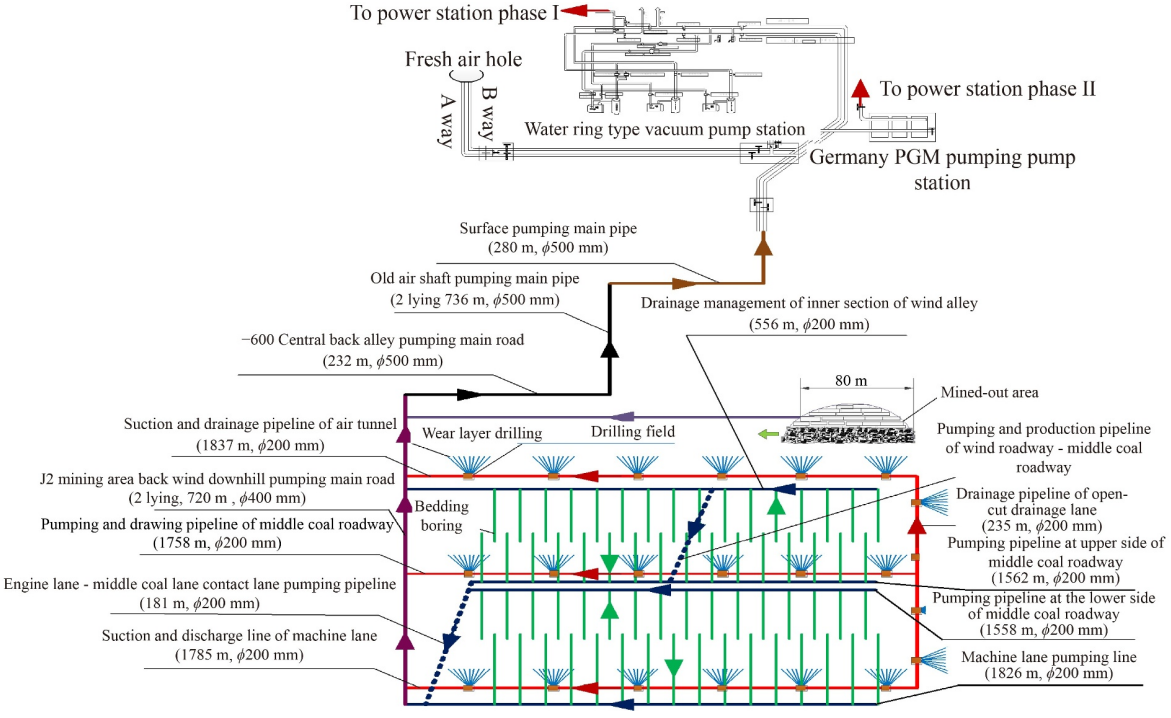

Fig. 8 Comprehensive pipeline system of gas three-dimensional drainage.

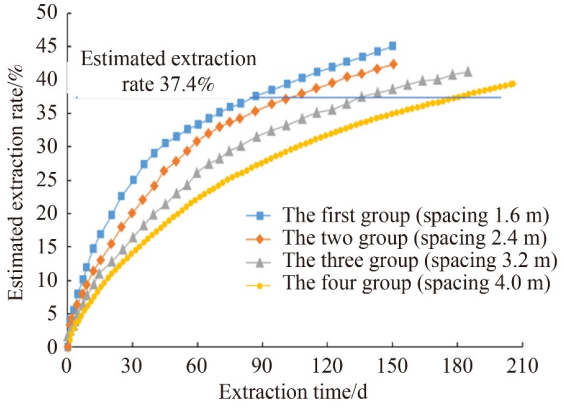

Fig. 9 Relation diagram of drilling time and pre-pumping rate of each group.

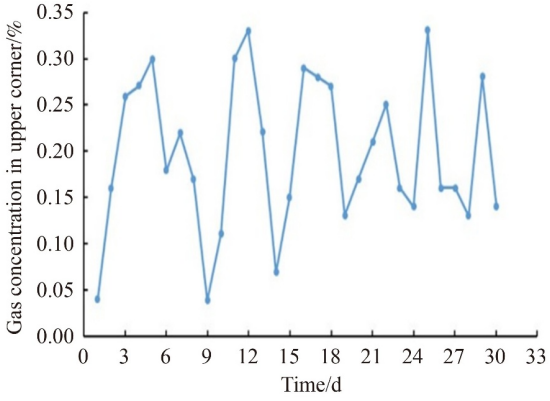

Fig. 10 Gas concentration in the upper corner of high drainage roadway during drainage.

To test the control effect of excess gas in the upper corner, the gas concentration in the upper corner of work face 12090 was monitored during the pumping period of the high-pumping roadway. The monitoring results are shown in Fig. 10. During the pumping period, the gas concentration in the upper corner was stable at 0.04%–0.33% without local excess, meeting gas control requirements for the work face corner.

To test the technical effect of the bottom drainage roadway, a group of boreholes within the bottom gas extraction lane were selected. In the gas drainage boreholes with different horizontal distances from the bottom, a flowmeter was installed to study the change in gas concentration over time (Fig. 11). Figure 12 shows the variation in gas concentration with different horizontal distances of 0, 20, and 30 m extraction from drilling.

Under the mining stress action, the drainage effect of the pre-drainage borehole in the bottom drainage roadway was remarkable. The gas drainage concentration of the borehole through the layer in the bottom drainage roadway reached stability in approximately 10 days under different horizontal distances. In the early stage of extraction, the gas concentration in boreholes at horizontal distances of 0, 20, and 30 m was 65%, 44%, and 40%, respectively. After 20 days, the gas concentration decreased to 20%, 10%, and 6%, respectively. After 30 days, the gas concentration decreased to 9%, 4%, and 2%, respectively. Under the influence of pressure relief in roadway excavation, the evolution of borehole gas concentration showed that the closer the borehole was to the floor roadway, the greater the extraction effect was. To examine the influence of different distances on the gas pressure in the coal seam, pressure measuring holes were

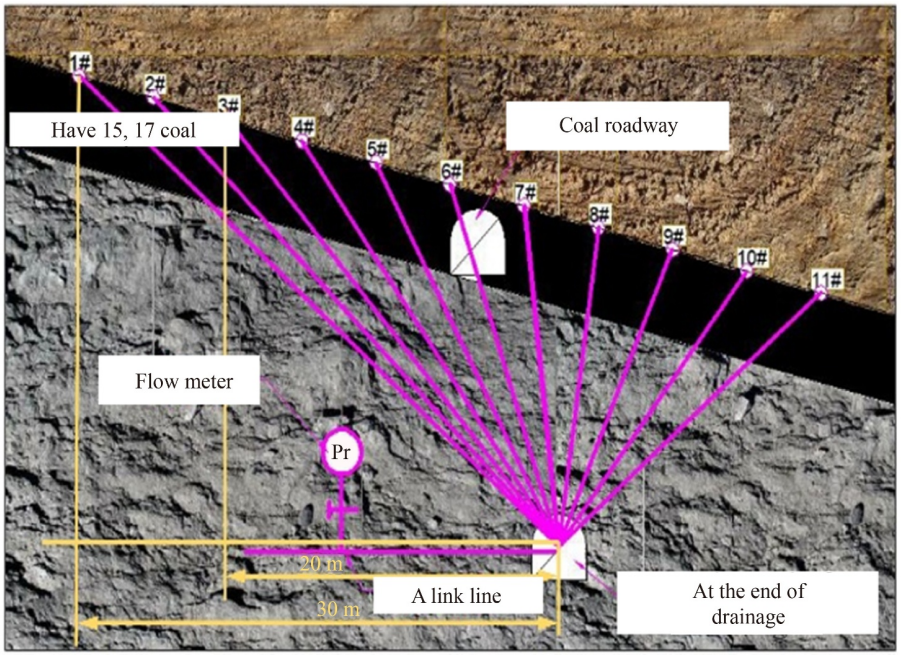

Fig. 11 Layout of gas drainage borehole in the bottom drainage roadway.

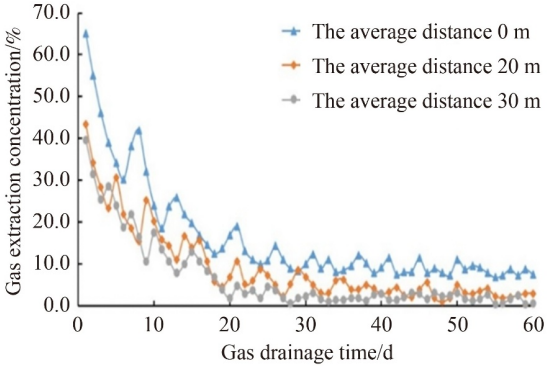

Fig. 12 Changes in gas concentration over time.

arranged in the special gas extraction lane of the floor, with 3 holes in each group and an intra-group spacing of 13 m. The inter-group spacing was 40 m and the bore diameter was 89 mm, as shown in Fig. 13.

To test the effect of gas pressure reduction in the coal seam, three groups of pressure-measuring boreholes were selected and the horizontal distances between the middle part and the bottom pumping roadway were 0, 20, and 30 m. The variation in gas pressure and residual gas pressure in the manometric borehole is shown in Fig. 14.

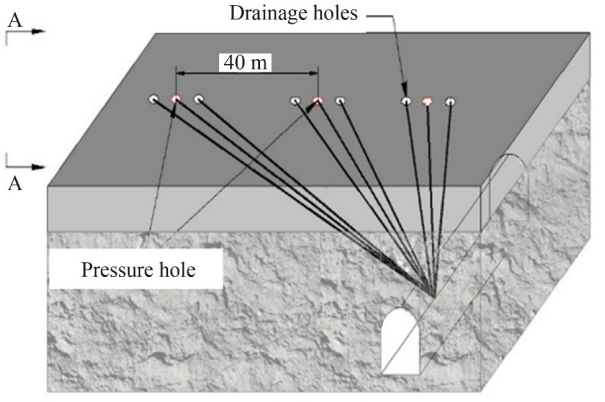

(a)

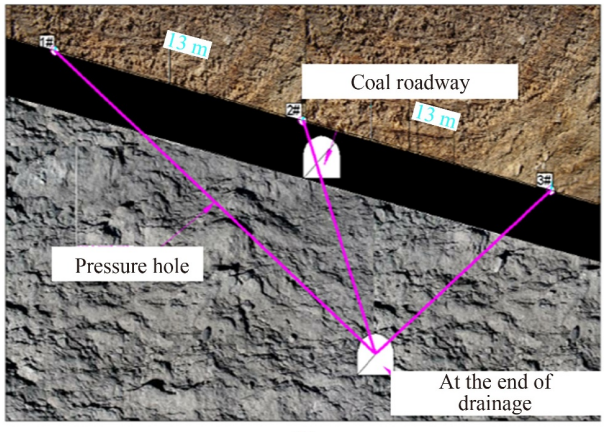

(b)

Fig. 13 Schematic diagram of pressure tap arrangement. (a) Layout of manometric borehole. (b) Layout plan of manometric borehole section.

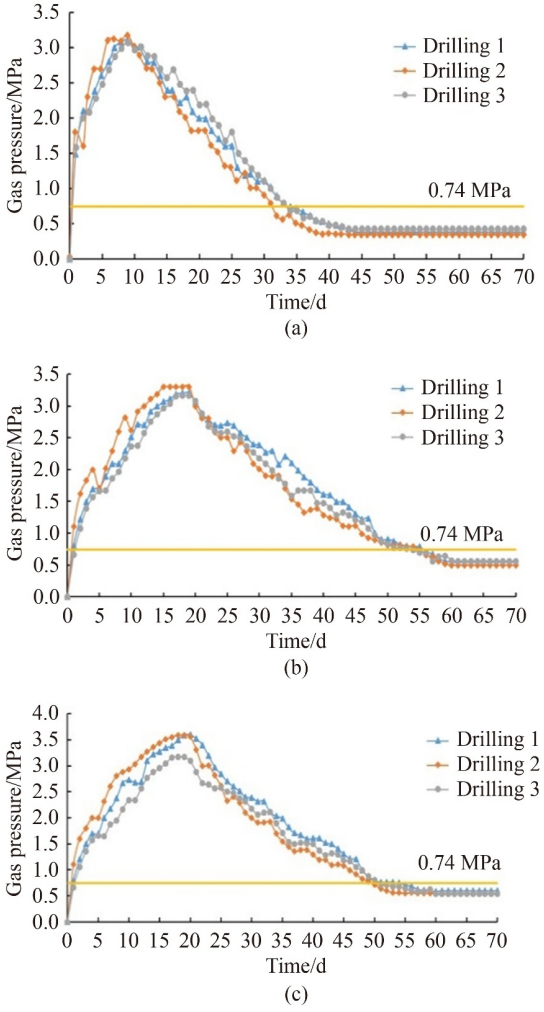

Fig. 14 Change in gas pressure in the coal seam over time in the pre-drainage area. (a) Change in gas pressure in borehole at 0 m horizontal distance with time. (b) Change in gas pressure with time at 20 m horizontal distance. (c) Change in gas pressure with time at 30 m horizontal distance.

Through the analysis of gas pressure monitoring data, the gas pressure of the coal seam at 0 m distance reached a stable peak of 3.3 MPa after 9 days. Following network drainage, the gas pressure gradually decreased to 2.4 MPa after 10-day drainage, 1.2 MPa after 20-day drainage, 0.74 MPa after 25-day drainage, and to a stable state of 0.4 MPa after 34-day drainage. This value was regarded as the residual gas pressure.

The gas pressure of the coal seam at 20 m reached a stable value of 0.6 MPa (residual gas pressure) after 50-day extraction, and the gas pressure of the coal seam at 30 m reached a stable value of 0.65 MPa (residual gas pressure) after 50-day extraction.

It took less than 16 days and 19 days for the coal seam gas pressure to reach the safe value of 0.74 MPa at the horizontal distance of 0 m compared with those at 20 and 30 m, respectively. The extraction effect of the borehole on the tile pressure of the coal seam was much higher

than that of the bottom pumping roadway at horizontal distances of 20 and 30 m.

As the original gas pressure increased from 3.5 MPa to 0.4 MPa during deep well mining and in the large mining height work face, field application of the three-dimensional coal seam gas extraction technology successfully increased the critical strength index of coal and rock mass by 39.13% (from 12.83 MPa to 17.85 MPa). Consequently, the risk of stress-induced dynamic disaster was reduced.

After treatment of the mining surface of 12090, the gas extraction volume increased, with a monthly maximum gas extraction volume of 3.45 million m^3, monthly maximum gas consumption of 2.72 million m^3, and electricity generation of 4.08 million kW·h. The daily maximum power generation reached 140000 kW·h, saving over 30 million RMB in electricity costs for the mine every year and reducing gas emissions by over 20 million m^3. The maximum daily production of the mining surface was increased from 6000 tons to 13000 tons, with a monthly production capacity of 260000 tons, and an annual production capacity of 3 million tons. Therefore, simultaneous extraction of coal and gas was achieved, which laid a foundation for safe and efficient production.

5 Conclusions

1) In the present study, the evolution of primary rock stress and mining-induced stress was systematically analyzed based on the geological characteristics of a deep gas outburst mine in the Pingdingshan mining area. The critical criterion of instability failure of coal and rock mass was established based on the theoretical framework of fracture mechanics and the mechanism of coupled instability failure of *in situ* stress and gas was analyzed.

2) Focusing upon the large mining face of the Shoushan mine, the original design was used as the basis to add the wind and transportation lanes for gas drainage and coal and gas drainage lanes for special gas drainage and special high gas drainage lanes, respectively. With the original coal lane serving as the ventilation lane, a seven-alley gas control technology for the coal seam was proposed. By optimizing the layout, a three-dimensional pumping system of one side and seven lanes was developed.

3) Focusing on the extraction system in Shoushan mine, a field test was conducted to investigate the drainage borehole layout parameters and the effective radius of extraction. We explored the drainage borehole and relationship between various parameters and the gas extraction effect. A method of large mining height coal seam gas solid extraction and the deep dynamic disaster management demonstration project were established.

4) Through the demonstration project, the gas content and pressure in the deep mine work face were effectively reduced. The critical strength of coal and rock mass instability and failure was increased, and the risk of dynamic disaster was reduced, which aided in solving corresponding problems for other mines.

5) In the calculation of critical strength index of coal and rock mass in this study, the friction coefficient was 0.5 when the sandstone was dry. If the lithology of the roof and floor changed or the rock mass was saturated, the friction coefficient dropped below 0.2 and the critical strength index decreased by 70%. Therefore, the drainage and depressurization in the deep well mining are important disaster prevention parameters that must be utilized.

Acknowledgments This study was financially supported by the National Natural Science Foundation of China (Grant No. 51874053), the Scientific Research Foundation of State Key Laboratory of Coal Mine Disaster Dynamics and Control (No. 2011DA105287-zd201804).

References

ASTM (1983). Standard test method for plane strain fracture toughness of metallic materials. Annual Book of ASTM Standards, Part 10, Philadelphia: American Society for Testing and Materials

Cao H (2009). Research on fracture toughness of high-grade pipeline steel for gas and oil. Dissertation for Master's Degree. Wuhan: Wuhan University of Technology

Deng H, Zhu M, Li J, Wang Y, Luo J, Yuan X (2012). Study of mode-I fracture toughness and its correlation with strength parameters of sandstone. Rock Soil Mech, 33(12): 71–77 (in Chinese)

Gong F, Lu D, Li X, Rao Q, Fu Z (2014). Toughness increasing or decreasing effect of hard rock fracture with pre-static loading under dynamic disturbance. Chinese J Rock Mech Eng, 33(9): 1905–1915 (in Chinese)

Kang H (2013). Stress distribution characteristics and strata control technology for roadways in deep coal mines. Coal Sci. Technol, 41(9): 12–17

Kuruppu M D, Obara Y, Ayatollahi M R, Chong K P, Funatsu T (2014). ISRM-suggested method for determining the mode I static fracture toughness using semi-circular bend specimen. Rock Mech Rock Eng, 47(1): 267–274

Li Y, Yang K, Qin R, Yu Y (2020). Technical system and prospect of safe and efficient mining of coal and gas outburst coal seams. Coal Sci Technol, 48(03): 167–173

Liu X, Liu Q, Liu B, He J (2018). Research on numerical method for crack propagation simulation with consideration of damage effect. Chinese J Rock Mech Eng, 37(S2): 64–72

Liu Y, Lebedev M, Zhang Y, Wang E, Li W, Liang J, Feng R, Ma R (2022). Micro-cleat and permeability evolution of anisotropic coal during directional CO_2 flooding: an *in situ* micro-CT study. Nat Resour Res, 31(5): 2805–2818

Lu Y (2018). Effect of bedding plane direction on fracture toughness of shale under different loading rates. Chinese J Rock Mech Eng, 37(6): 1359–1370 (in Chinese)

Ma L, Cao H, Zhang Z, Gao Q, Luo Z (2019). An experimental investigation of the fracture behaviors of type-I cracks in shales with different bedding angles. Petrol Sci Bull, 4(04): 347–353 (in Chinese)

Qi Q, Pan Y, Shu L, Li H, Jiang D, Zhao S, Zou Y, Pan J, Wang K, Li H (2018). Theory and technical framework of prevention and control with different sources in multi-scales for coal and rock dynamic disasters in deep mining of coal mines. J China Coal Soc, 43(07): 1801–1810 (in Chinese)

Srawley J E, Brown W F (1965). Fracture toughness testing methods. ASTM Spec Tech Publ, 381: 133–145

Tian J, Wang L, Cheng Y, Ma X, Li W, Shen Z (2008). Research on distribution rule and forecast method of gas pressure in coal seam. J Min Safety Eng, 25(4): 481–485 (in Chinese)

Whittaker B N, Singh R N, Sun G (1992). Rock Fracture Mechanics: Principles, Design and Applications. Amsterdam: Elsevier

Xie H, Gao F, Ju Y, Gao M, Zhang R, Gao Y, Liu J, Xie L (2015). Quantitative definition and investigation of deep mining. J China Coal Soc, 40(01): 1–10 (in Chinese)

Yan B (2010). Experimental study on reasonable parameters of gas pre-drainage in coal seam. Energy Tech Manag, 5: 32–34 (in Chinese)

Zhang B, Yang S, Kang L, Zhai Y (2008). Discussion on method for determining reasonable position of roadway for ultra-close multi-seam. Chinese J Rock Mech Eng, 1: 97–101 (in Chinese)

Zhang J G (2015). Geostress measurement technology by rheological stress recovery method and its application. Safety in Coal Mines, 46(S1): 34–38 (in Chinese)

Zhang J G, Lan T W, Wang M, Gao M Z, Rong H (2019). Prediction method of deep mining dynamic disasters and its application in Pingdingshan mining area. J China Coal Soc, 44(6): 1698–1706 (in Chinese)

Zhang J, Song Z (2020). Mechanical response and failure characteristics of deep sandstone under triaxial loading and unloading. J Min Safety Eng, 37(2): 409–418+428

Zhang Z X, Kou S Q, Lindqvist P A, Yu Y (1998). The relationship between the fracture toughness and tensile strength of rock. In: Strength Theories: Applications, Evelopment & Prospects for 21st Century. Beijing/NewYork: Science Press

Zhu L, Li Z, Liu H (2017). Consequential mechanism and the monitoring technique for the gassy coal-rock dynamics disaster in the deep mining. J Safety Environ, 17(03): 937–942 (in Chinese)